analytical chemistry

pubs.acs.org/ac Article

Imaging of Hydroxyl-Radical Generation Using Dynamic Nuclear Polarization-Magnetic Resonance Imaging and a Spin-Trapping Agent

Shinichi Shoda, Fuminori Hyodo,* Yoko Tachibana, Mamoru Kiniwa, Tatsuya Naganuma, Hinako Eto, Norikazu Koyasu, Masaharu Murata, and Masayuki Matsuo

Cite This: https://dx.doi.org/10.1021/acs.analchem.0c02331 Read Online

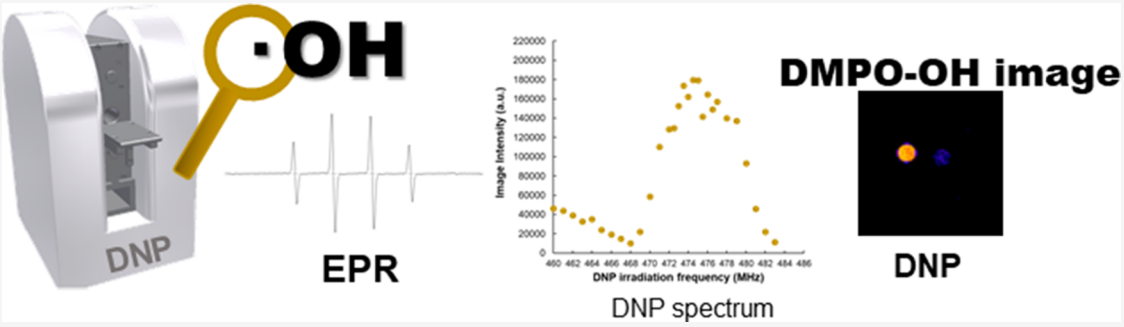

ABSTRACT: Reactive oxygen species (ROS) play an important role in cell metabolism, but they can cause oxidative damage to biomolecules. Among ROS, the hydroxyl radical (·OH) is one of the most reactive molecules in biological systems because of its high reaction rate constant. Therefore, imaging of ·OH could be useful for evaluation of the redox mechanism and diagnosis of oxidative diseases. In vivo dynamic nuclear polarization-magnetic resonance imaging (DNP-MRI) is a noninvasive imaging method to obtain spatiotemporal information about free radicals with MRI anatomical resolution. In this study, we investigated the visualization of hydroxyl radicals generated from the Fenton reaction by combining DNP-MRI with a spin-trapping agent (DMPO: 5,5-dimethyl-1-pyrroline *N*-oxide) for ·OH. Additionally, we demonstrated the radical-scavenging effect using four thiol-related reagents by DNP-MRI. We demonstrated that DNP enhancement could be induced by the DMPO-OH radical using the DNP-MRI/spin-trapping method and visualized ·OH generation for the first time. Maximum DNP enhancement was observed at an electron paramagnetic resonance irradiation frequency of 474.5 MHz. Furthermore, the radical-scavenging effect was simultaneously evaluated by the decrease in the DNP image value of DMPO-OH. An advantage of our methods is that they simultaneously investigate compound activity and the radical-scavenging effect.

■ INTRODUCTION

Reactive oxygen species (ROS) are produced during both normal and abnormal cellular metabolism and can play both beneficial and harmful roles in cell physiology. The beneficial effect of ROS is that they act as messengers in cell-signaling pathways and inflammatory responses, such as infusion of neutrophils for production of superoxide via NADPH oxidase.[1] However, ROS also have harmful effects, including oxidative damage to biomolecules such as lipids, proteins, nucleic acids, and sugars.[2,3] This oxidative stress might induce when the balance between ROS generation and the antioxidant defenses is shifted toward more oxidizing conditions. Oxidative stress has been implicated in a variety of diseases, such as neurodegenerative disorders, atherosclerosis, diabetes, inflammation, and cancer.[4−7] Among ROS, the hydroxyl radical (·OH) is one of the most reactive molecules in biological systems because of its high reaction rate constant.[8−10] Therefore, monitoring of ·OH could be useful for evaluation of the redox mechanism and diagnosis of oxidative diseases.

Many studies have reported the detection of ·OH generation with high sensitivity using methods such as the fluorescent probe method and chemiluminescence.[11−13] However, these methods are difficult to use for in vivo studies because of limitations surrounding the permeability of fluorescence wavelengths (less than 1 mm), and they also provide no direct evidence of free-radical detection. Electron paramagnetic resonance (EPR) spectroscopy with a spin-trapping agent is a

Received: June 1, 2020
Accepted: October 6, 2020

convenient and useful technique to detect free radicals and identify ROS by their spectral signals.[14,15] In this technique, short-lived oxygen-derived radicals are trapped by a spin-trapping agent to form long-lived radicals and generate an EPR spectrum. One of the most recognized spin-trapping agents is 5,5-dimethyl-1-pyrroline *N*-oxide (DMPO), whose spin adduct generates a hydroxyl radical-specific EPR spectrum as DMPO-OH (Figure 1B).[16] Therefore, imaging of hydroxyl-radical generation enables monitoring of ROS generation and the antioxidant activity of chemical drugs in oxidative disease. However, because the image resolution of EPR imaging is directly dependent upon the linewidth of free-radical compounds, EPR images' spatial resolution is relatively low. Additionally, fast imaging is needed for visualization of spin-trapped free radicals because of the instability of spin-trapped adducts. Therefore, EPR imaging technology has not yet achieved this type of visualization. Recently, Saito et al. performed biological imaging using ^{13}C-labeled DMPO using hyperpolarized NMR.[17] They clearly visualized DMPO metabolism, but they did not show the distribution of DMPO-OH.

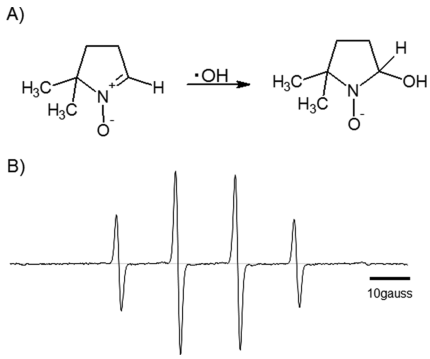

Figure 1. Chemical structure of 5,5-dimethyl-1-pyrroline *N*-oxide (DMPO) and DMPO-OH and the EPR spectrum of DMPO-OH. (A) Chemical structure of DMPO and its spin adduct, DMPO-OH. (B) EPR spectra of DMPO-OH produced by the hydroxyl-radical generation system (Fenton reaction).

In vivo dynamic nuclear polarization-magnetic resonance imaging (DNP-MRI) is a noninvasive imaging technology to obtain spatiotemporal information about free radicals and redox status with the anatomical resolution of MRI.[18,19] The proton signal in tissues includes free radicals, as the DNP effect can be dramatically enhanced by EPR irradiation at the resonant frequency of the free radical prior to applying the MRI pulse sequence. Therefore, DNP-MRI has been used to investigate the functional status of tissues, such as their redox state,[20,21] oxygen partial pressure,[22] and malignant ascites[23] using redox-sensitive nitroxyl radicals. In this study, we investigated the visualization of hydroxyl radicals by combining DNP-MRI with spin trapping of hydroxyl radicals using DMPO and visualization of the radical-scavenging effects by DNP imaging of DMPO-OH.

■ MATERIALS AND METHODS

Chemicals. We purchased DMPO from Dojindo Laboratories, and ferrous sulfate heptahydrate and phorbol 12-myristate13-acetate (PMA) were purchased from Wako. Suplatast tosilate (ST) was purchased from Tokyo Chemical Industry Co., Ltd. (Tokyo Japan) All other chemicals were commercially available and of reagent-grade quality. All reagents and solvents were of analytical grade, unless otherwise specified, and used without further purification. Water was purified with a Milli-Q system from Millipore (Nihon Millipore K.K., Tokyo, Japan).

Fenton Reaction and Spin-Trapping Assay. Hydroxyl radicals were generated by the Fenton reaction and trapped with DMPO.[24,25] In the Fenton reaction, iron(II) was oxidized by H_2O_2 to iron(III), generating a hydroxyl radical and a hydroxide ion. The DMPO-OH adduct was obtained by mixing a DMPO solution with H_2O_2 and $FeSO_4$ to a final volume with PBS. The DMPO, H_2O_2, and $FeSO_4$ final concentrations used ranged 10−400 mM, 1−400 mM, and 4−5 mM, respectively.

Detection of Hydroxyl Radicals with DMPO by X-Band EPR Experiments. EPR spectra were obtained with an X-band EPR spectrometer (JEOL Ltd. Tokyo, Japan) at room temperature under the following conditions: microwave frequency = 9.4 GHz (336 mT); microwave power = 1 mW; modulation width = 0.06 mT; sweep time = 1 min; sweep width = ±5 mT; and time constant = 0.03 s. The reaction mixture contained the following reagents and final concentrations: 10 mM DMPO, 5 mM H_2O_2, and 5 mM $FeSO_4$. The EPR spectrum was recorded 1 min after the reagents were mixed.

Phantom Imaging of DMPO-OH Using DNP-MRI. In vitro free-radical imaging was performed with a low-field DNP−MRI system (Keller) obtained from Japan Redox Inc. (Fukuoka, Japan). The external magnetic field (B_0) for EPR irradiation and MRI was fixed at 15 mT, and the radio-frequency of the EPR irradiation ranged 460−483 MHz. As a high-sensitivity local detector, a rectangular round surface coil (longitudinal direction 20 mm, lateral direction 20 mm) was used for EPR irradiation.

In DNP-MRI, the DNP phenomenon is induced by irradiating a resonant microwave adjusted to the resonant frequency of the electron spin of the free-radical solution. Therefore, it is necessary to determine the suitable resonant frequency of the DMPO-OH radical for induction of DNP. A phantom (200 μL, 5.4 mm inner diameter, and 9 depth) was prepared for comparison of the DNP phenomenon. In the left tube of the phantom, DMPO solution was added after H_2O_2 and $FeSO_4$ were mixed. The final concentrations of DMPO, H_2O_2, and $FeSO_4$ were 400, 400, and 4 mM, respectively. Another tube inside the phantom was filled with PBS. A surface coil for EPR irradiation and a DNP−MRI system were used to obtain the phantom images. To determine the optimum EPR-resonant frequency of DMPO-OH, DNP-MRI measurements were performed while changing the EPR irradiation frequency in steps of 0.5 MHz or 1 MHz from 460 to 483 MHz. The phantom images were obtained by DNP-MRI 30 s after mixing the H_2O_2 and $FeSO_4$. The scanning conditions for the DNP-MRI were as follows: power of EPR irradiation = 7 W; flip angle = 90°; repetition time (TR) × echo time (TE) × TEPR = 500 × 25 × 250 ms; number of acquisitions = 10; and number of phase-encoding steps = 32. The image's field of view (40 × 40 mm) was represented by 64 × 64 matrix after image reconstruction.

Effects of H_2O_2 Concentration on DNP-MRI. Various concentrations of H_2O_2 (1−400 mM) and a constant concentration of $FeSO_4$ (4 mM) were mixed in a four-tube phantom (200 μL, 5.4 mm deep, and 9 mm depth) to investigate the effect of H_2O_2, and then DMPO (0.4 M) was

https://dx.doi.org/10.1021/acs.analchem.0c02331
Anal. Chem. XXXX, XXX, XXX−XXX

added. The EPR irradiation frequency was set to 474.5 MHz for DNP−MRI measurement. DNP−MRI measurements were performed 90 s after mixing of DMPO. The scanning conditions for the DNP−MRI experiment were as follows: EPR irradiation power = 7 W; flip angle = 90°; TR × TE × TESR = 500 × 25 × 250 ms; and number of acquisitions = 10.

Imaging of Neutrophil-Derived DMPO-OH. A total of 1.2 mL of 4% thioglycollate (TGC) medium (Nissui Pharmaceutical) was injected into the peritoneum of female Slc: ICR mice.[26] Peritoneal cells were harvested by lavage with Hanks Balanced Salt Solution at 4 h after injection. Cells were collected by centrifugation at 1000 × g for 5 min at 4 °C, and the supernatant was removed. The neutrophils (4.0×10^7 cells/mL) were mixed with DMPO (700 mM) and PMA (0.01 mM) and incubated at 37 °C for 1 min. Imaging was performed by DNP-MRI 3 min after mixing.

Imaging of the Hydroxyl Radical-Scavenging Effect. As antioxidants for hydroxyl-radical generation, we employed thiols such as dimethyl sulfoxide (DMSO), dimethyl sulfone (DMS), dimethyl sulfoniopropionate (DMSP), and ST. The known hydroxyl-radical-scavenging effect of DMSO[27] was compared with the inhibitory effects of the other thiols above by EPR, and we confirmed the visualization of those effects using DNP-MRI. Various concentrations of those compounds were mixed with Fenton reagents, and the EPR signal and image intensity were observed by DNP-MRI. The thiol compounds were added to a mixed solution of DMPO, H_2O_2, and $FeSO_4$ in a four-tube phantom.

The concentrations of the solutions subjected to EPR measurement were 10, 5, and 5 mM for DMPO, H_2O_2, and $FeSO_4$, respectively. The corresponding concentrations were 400, 400, and 5 mM for DMPO, H_2O_2, and $FeSO_4$, respectively. The concentrations of all other thiol compounds were 2.5 mM. The ESR and DNP-MRI measurements were performed 30 s after mixing of H_2O_2 and $FeSO_4$. The scanning conditions for the DNP−MRI experiment were as follows: EPR irradiation frequency = 474.5 MHz; EPR irradiation power = 7 W; flip angle = 90°; TR × TE × TESR = 500 × 20 × 250 ms; number of acquisitions = 1; slice thickness = 100 mm; field of view = 40 mm; and sampling number = 64. The inhibition map was calculated using the following formula: Inhibition map = (1 − Image intensity (DNP on) /Image Intensity (PBS)) × 100.

■ RESULTS AND DISCUSSION

Figure 1 shows the chemical structure and EPR spectrum of DMPO-OH, which is the spin-trapping adduct of DMPO and ·OH. It is known that the spin-trapping agent, DMPO, could react with the ·OH produced by the Fenton reaction and be converted to DMPO-OH, which produces the EPR spectrum. The EPR spectrum of DMPO-OH has four peaks (ratio of peak heights is 1:2:2:1); therefore, the production of ·OH generation could be identified by the form of the spectrum. To determine the appropriate EPR-resonant frequency of the DMPO-OH free radical for obtaining the DNP effect, DNP-MRI was performed at various EPR frequencies from 460 to 483 MHz (Figure 2 and Figure S1). Figure 2A shows typical examples of DNP images of DMPO-OH at various EPR frequencies. Imaging with DMP-MRI clearly visualized the enhancement of phantom tubes, including the hydroxyl-radical generation system between 471 and 480 MHz. Although the DNP enhancement in the tube including the DMPO-OH showed no enhancement at EPR irradiation frequencies from

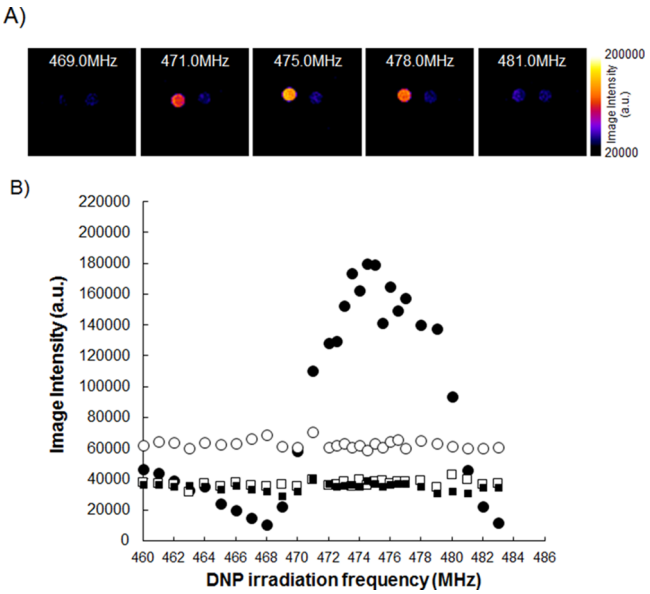

Figure 2. Determination of suitable EPR frequencies of DMPO-OH for DNP enhancement. (A) DNP images at various EPR irradiation frequencies at 30 s after mixing the DMPO and Fenton reagents. In each case, the left tube contains DMPO-OH, and the right tube was filled with PBS. (B) Plots of DNP image intensity at various EPR frequencies. DNP-MRI was performed at various EPR frequencies from 460 to 483 MHz. Image intensity of DMPO-OH including tubes with (closed circle) or without (open circle) EPR irradiation. Image intensity of the PBS tube with (closed square) or without (open square) EPR irradiation.

460 to 469 MHz, enhancement was increased above 470 MHz (Figure 2B). Maximum enhancement was observed at 474.5 MHz, and then the enhancement decreased at higher frequencies. The enhancement factor (DNP on/DNP off) was 3.07 at 474.5 MHz. In contrast, in DMPO-OH solutions that did not receive EPR irradiation, the MRI signal did not change. In tubes filled with PBS, the MRI signal always showed no enhancement regardless of the frequency or presence of EPR irradiation. The image intensity of DMPO-OH solutions without EPR irradiation was higher than that of PBS solutions because of the T_1 shortening of $FeSO_4$ in the ·OH generation system. These results suggested that the DMPO-OH radical induces the DNP and generates an enhancement image using the DNP−MRI system and that the optimal frequency is 474.5 MHz.

Next, we examined the dependence of DNP−MRI signal enhancement on the H_2O_2 concentration (Figure 3A). As expected, enhancement was positively associated with the H_2O_2 concentration (Figure 3B). We also confirmed negative enhancement at lower H_2O_2 concentrations, which we also observed previously.[19] In these DNP−MRI experiments, we could not use high concentrations of $FeSO_4$ to increase the generation of ·OH because $FeSO_4$ decreases the T_1 relaxation time and also decreases the image intensity on regular MRI at higher concentrations. No effect of $FeSO_4$ on DNP-MRI at 16 mT was observed at concentrations up to 4 mM. Therefore, we used a 4 mM $FeSO_4$ solution in the Fenton reaction. In addition, we observed enhancement by the activated neutrophil-derived DMPO-OH on EPR and DNP−MRI studies (Figure 3C). DNP enhancement on the DNP ON image in phantom including activated neutrophils and DMPO was observed compared to the DNP OFF image. The EPR

https://dx.doi.org/10.1021/acs.analchem.0c02331
Anal. Chem. XXXX, XXX, XXX−XXX

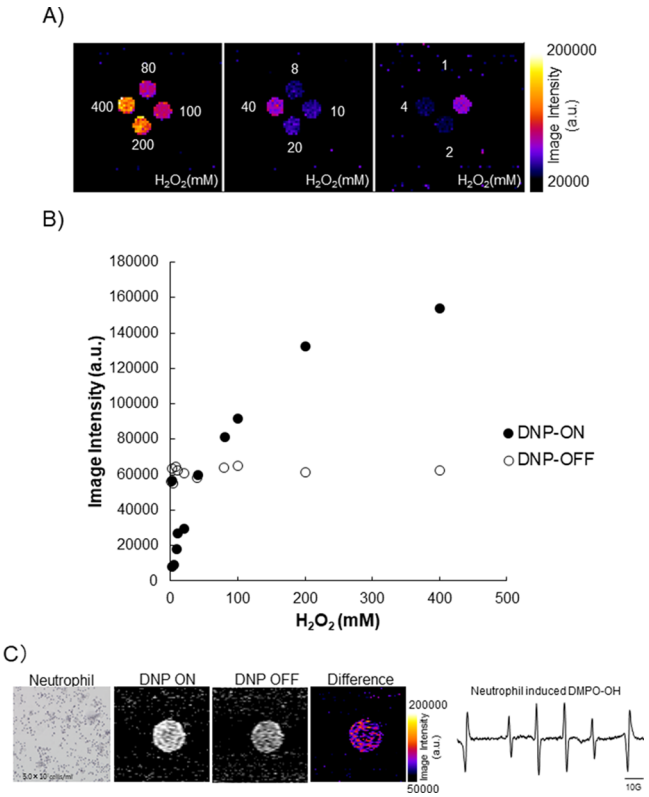

Figure 3. DNP enhancement by modulation of H_2O_2 concentration in DNP-MRI and imaging of neutrophil-derived DMPO-OH. (A) DNP images of phantoms filled with various concentrations of H_2O_2, acquired by DNP-MRI at 475 MHz. (B) Plots of DNP image intensity with various H_2O_2 concentrations. (C) Imaging of activated neutrophil-derived DMPO-OH. Neutrophils were collected from mouse abdomen 4 hr after TGC treatment. DNP-MRI and EPR spectroscopy were performed 1 min after incubation of neutrophils with PMA and DMPO.

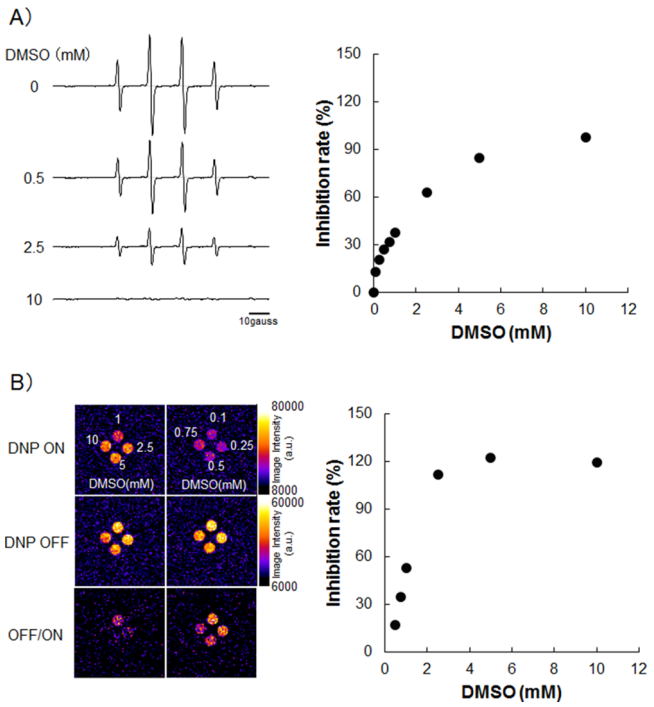

Figure 4. Visualization of the radical-scavenging effect of DMPO on the hydroxyl-radical generation system using DNP-MRI. (A) EPR spectra of DMPO-OH and its inhibition rate after treatment with various concentrations of DMSO. (B) Enhanced DNP images and inhibition rates of DMPO-OH treated with various concentrations of DMSO obtained by DNP-MRI. All tubes included 10 mM DMPO, 5 mM H_2O_2, and 5 mM $FeSO_4$. DMSO (0, 0.1, 0.25, 0.5, 0.75, 1, 2.5, 5, or 10 mM) was added as a radical scavenger.

spectrum of DMPO-OH in a neutrophil suspension with DMPO was also observed. It is known that DMPO-OH is generated from DMPO-OOH decomposition in the neutrophil-induced ROS and DMPO system.[28,29] In this study, we demonstrated that the endogenously produced DMPO-OH from the cells could be imaged by DNP-MRI.

To investigate the imaging of the scavenging effect by DNP-MRI, we used DMSO, which has an ·OH-scavenging effect[27] in the ·OH generation system. At first, an EPR study was performed to confirm the inhibition effect of DMSO against ·OH generation (Figure 4A). The EPR signal decreased with increasing DMSO concentration, and it was completely inhibited by 10 mM DMSO. In the DNP−MRI experiments, DMSO had a similar effect (Figure 4B). Although the image intensities of the phantom were almost the same value with DNP off, the image intensity with DNP on decreased with the addition of DMSO. At 5 mM DMSO, enhancement was completely suppressed. These results suggest that DNP-MRI can detect the radical-scavenging effect and might be useful for simultaneous imaging of various samples to confirm radical-scavenging ability.

The sulfur biochemistry of the thiol group has unique features, and highly abundant low-molecular-weight thiol counterparts are carefully balanced to maintain the redox homeostasis in various cellular compartments, protecting organisms from oxidative stress.[30] Therefore, the role of thiol redox biology has become more important in the development of understanding about the redox regulation system and signal processes. Thiol compounds have antioxidant capabilities to reduce oxidative stress.[31] In this study, we selected the thiol compounds to simultaneously observe their radical-scavenging effects by DNP-MRI. Figure 5A shows the thiol compounds used for EPR and DNP-MRI in this study. First, the radical-scavenging effects of these thiol compounds were compared by EPR spectroscopy.

In the EPR spectroscopy experiment (Figure 5B), ST showed the strongest inhibition effect against hydroxyl-radical generation. The inhibition rates of DMSO, DMS, DMSP, and ST were 60, 2, 40, and 90%, respectively. DMSP and DMS showed lower inhibition effects than DMSO. In the DNP−MRI experiment (Figure 5C), the inhibitory effects were compared in the images acquired by DNP-MRI, and the difference images clearly showed the inhibition-dependent manner of the thiol compounds' action. Enhancement by DMPO-OH on ST images including phantom was significantly lower than that of the other thiols. This suggests that ST suppressed the production of DMPO-OH and reduced the effects of DNP in DNP-MRI.

It is possible for DNP-MRI to simultaneously visualize radical-scavenging effects in multiple samples, including various thiol compounds. Although DMSO has a strong ·OH radical-scavenging effect,[27] in this experiment, ST more effectively suppressed DMPO-OH production. In Japan, ST is widely used as an oral asthma control drug and has been prescribed to adults and pediatric patients with allergic rhinitis and atopic dermatitis for more than 20 years.[32−34] Recently,

https://dx.doi.org/10.1021/acs.analchem.0c02331
Anal. Chem. XXXX, XXX, XXX−XXX

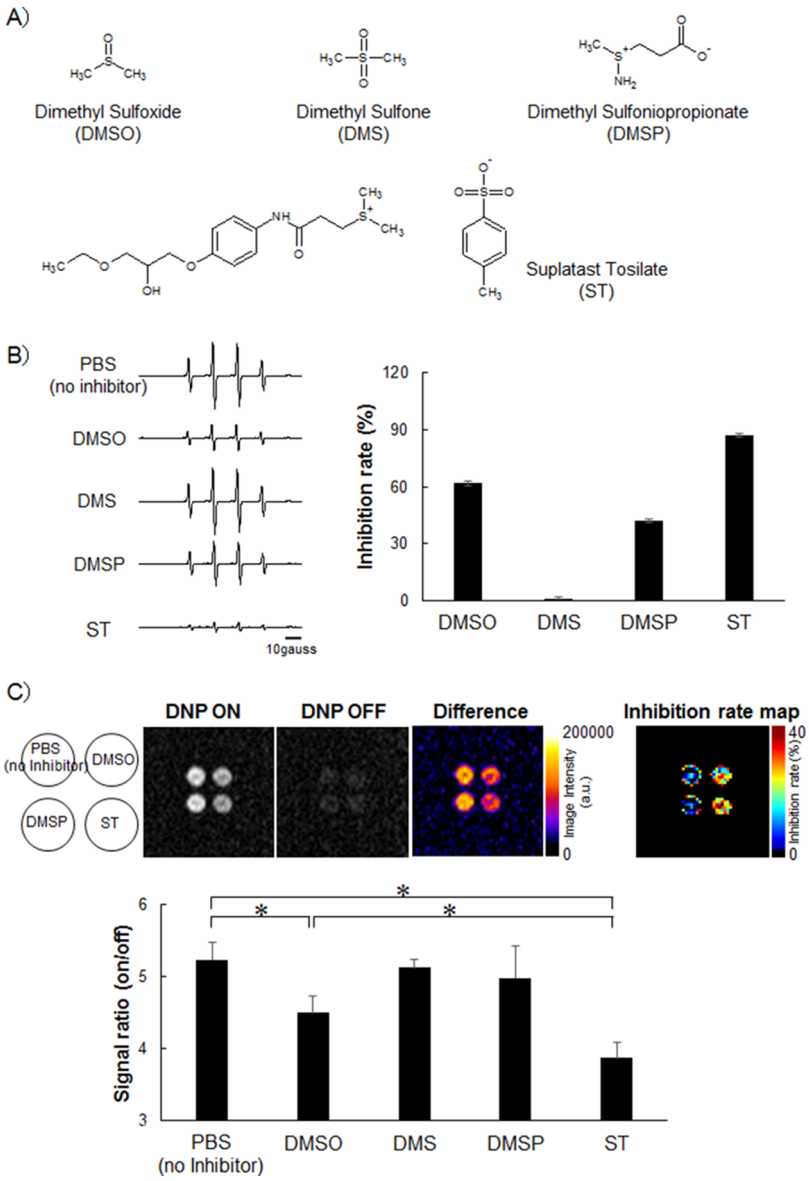

Figure 5. Simultaneous imaging of the hydroxyl-radical-scavenging effect of various thiol compounds using EPR and DNP-MRI. (A) Chemical structures of thiol compounds. (B) EPR spectra and inhibition rates of DMPO-OH by various thiol compounds. All tubes included 10 mM DMPO, 5 mM H_2O_2, and 5 mM $FeSO_4$. The concentration of each thiol compound was 2.5 mM. (C) Simultaneous DNP imaging of DMPO-OH and the inhibition rate map in DMPO-OH tubes including various thiol compounds (*, $P < 0.05$). All tubes included 400 mM DMPO, 400 mM H2O2, and 4 mM FeSO4. The concentration of each thiol compound was 2.5 mM.

Izumi et al. reported that administration of ST reduced oxidative stress in radiation-induced lung injury and suppressed inflammation and fibrosis in mice.[35] They suggested that ST might also be useful as an antioxidant in the treatment of oxidative stress-mediated diseases. Additionally, Fukuhara et al. reported that ST protected the lungs against oxidative stress induced by hyperoxic exposure and prolonged the survival of mice exposed to hyperoxia.[36] They demonstrated that ST has an ·OH-scavenging effect using an EPR spin-trapping method with DMPO as a reference trapping agent. In our experiments, ST showed a strong radical-scavenging effect, even better than that of DMSO. An advantage of our methods is that they simultaneously evaluate the activity of compounds needed to investigate the radical-scavenging effect in this case.

In this study, we demonstrated that DNP-MRI could visualize the generation of ·OH as a DMPO-OH free radical and could evaluate the antioxidant efficacy in multiple samples. However, we used a high concentration of H_2O_2 to investigate the possibility of detection of hydroxyl-radical imaging by the DNP−MRI system. Therefore, it is necessary to increase the sensitivity of DNP-MRI or increase the averaging using long-live spin-trapping agents for application in living organisms.

A relatively high dose of H_2O_2 has been used in the Kochi oxydol-radiation therapy for treatment of the unresectable carcinomas (KORTUC) II radiosensitizer.[37,38] Linear accelerator-based stereotactic radiotherapy has little effect on most advanced neoplasms. The novel KORTUC II radiosensitizer, which contains H_2O_2 and sodium hyaluronate, was developed to address this shortcoming. The effectiveness of KORTUC II for the treatment of chemotherapy-resistant supraclavicular lymph node metastases, recurrent breast cancer, and stage-IV primary breast cancer has previously been demonstrated.[39−41]

https://dx.doi.org/10.1021/acs.analchem.0c02331
Anal. Chem. XXXX, XXX, XXX−XXX

Because KORTUC II administers radiation therapy after injecting a drug containing H_2O_2 into the tumor tissue, it is assumed that there is a high concentration of H_2O_2 in the tumor region. Therefore, our methodology might be used to understand the localization of radicals within the treatment site by administration of DMPO. The clinical application of this method is expected to expand to new theranostics that sensitizes the effects of radiation therapy and simultaneously visualizes the treatment area.

In conclusion, we succeeded in visualizing hydroxyl radicals using DNP-MRI and further showed that the hydroxyl-radical-scavenging effect could be evaluated using DNP-MRI.

■ ASSOCIATED CONTENT

Supporting Information

The Supporting Information is available free of charge at https://pubs.acs.org/doi/10.1021/acs.analchem.0c02331.

DNP enhancements observed between 470 MHz and 480 MHz for determining the appropriate EPR-resonant frequency of the DMPO-OH radical (PDF).

■ AUTHOR INFORMATION

Corresponding Author

Fuminori Hyodo − *Department of Radiology, Frontier Science for Imaging, School of Medicine, Gifu University, Gifu 501-1194, Japan; Innovation Center for Medical Redox Navigation, Kyushu University, Fukuoka 812-8582, Japan;* orcid.org/0000-0002-9266-9937; Phone: +81-58-230-6437; Email: hyodof@gifu-u.ac.jp; Fax: +81-58-230-6440

Authors

Shinichi Shoda − *Department of Radiology, Gifu University, Gifu 501-1194, Japan*

Yoko Tachibana − *Innovation Center for Medical Redox Navigation and Center for Advanced Medical Innovation, Kyushu University, Fukuoka 812-8582, Japan*

Mamoru Kiniwa − *Innovation Center for Medical Redox Navigation, Kyushu University, Fukuoka 812-8582, Japan*

Tatsuya Naganuma − *Japan Redox Limited, Fukuoka 812-0044, Japan*

Hinako Eto − *Innovation Center for Medical Redox Navigation and Center for Advanced Medical Innovation, Kyushu University, Fukuoka 812-8582, Japan*

Norikazu Koyasu − *Department of Radiology, Gifu University, Gifu 501-1194, Japan*

Masaharu Murata − *Innovation Center for Medical Redox Navigation and Center for Advanced Medical Innovation, Kyushu University, Fukuoka 812-8582, Japan*

Masayuki Matsuo − *Department of Radiology, Gifu University, Gifu 501-1194, Japan*

Complete contact information is available at: https://pubs.acs.org/10.1021/acs.analchem.0c02331

Notes

The authors declare no competing financial interest.

■ ACKNOWLEDGMENTS

This work was supported by the Medical Research and Development Programs Focused on Technology Transfer, Development of Advanced Measurement and Analysis Systems (SENTAN) from the Japan Agency for Medical Research and Development, AMED Grant Number 162128; a Health Labour Sciences Research Grant (Research on Publicly Essential Drugs and Medical Devices) from the Ministry of Health, Labour and Welfare of Japan; and Special Coordination Funds for Promoting Science and Technology (SCF funding program "Innovation Center for Medical Redox Navigation"). This work was also supported by JSPS KAKENHI (Grant Numbers 18H02765 and 19H03358). We thank Richard Lipkin, PhD, from Edanz Group (www.edanzediting.com/ac) for editing a draft of this manuscript.

■ REFERENCES

(1) Winterbourn, C. C.; Kettle, A. J.; Hampton, M. B. *Annu. Rev. Biochem.* **2016**, *85*, 765−792.
(2) Liochev, S. I. *Free Radical Biol. Med.* **2013**, *60*, 1−4.
(3) Lushchak, V. I. *Chem.-Biol. Interact.* **2014**, *224*, 164−175.
(4) Termini, J. *Mutat. Res.* **2000**, *450*, 107−124.
(5) Beckman, K. B.; Ames, B. N. *Physiol. Rev.* **1998**, *78*, 547−581.
(6) van Dam, P. S. *Diabetes/Metabol. Res. Rev.* **2002**, *18*, 176−184.
(7) Vendemiale, G.; Grattagliano, I.; Altomare, E. *Int. J. Clin. Lab. Res.* **1999**, *29*, 49−55.
(8) Bedjanian, Y.. *J. Phys. Chem. A* 2020.
(9) Toyokuni, S. *Cancer Sci.* **2009**, *100*, 9−16.
(10) Reyhani, A.; McKenzie, T. G.; Fu, Q.; Qiao, G. G. *Macromol. Rapid Commun.* **2019**, *40*, No. e1900220.
(11) Wardman, P. *Free Radical Biol. Med.* **2007**, *43*, 995−1022.
(12) Zamojc, K.; Zdrowowicz, M.; Jacewicz, D.; Wyrzykowski, D.; Chmurzynski, L. *Crit. Rev. Anal. Chem.* **2016**, *46*, 160−169.
(13) Lei, K.; Sun, M.; Du, L.; Zhang, X.; Yu, H.; Wang, S.; Hayat, T.; Alsaedi, A. *Talanta* **2017**, *170*, 314−321.
(14) Gomez-Mejiba, S. E.; Ramirez, D. C. *Mutat. Res.* **2019**, *782*, 108283.
(15) Mason, R. P. *Redox Biol.* **2016**, *8*, 422−429.
(16) Ranguelova, K.; Mason, R. *Magn. Reson. Chem.: MRC* **2011**, *49*, 152−158.
(17) Saito, K.; Sail, D.; Yamamoto, K.; Matsumoto, S.; Blackman, B.; Kishimoto, S.; Brender, J. R.; Swenson, R. E.; Mitchell, J. B.; Krishna, M. C. *Free Radical Biol. Med.* **2019**, *131*, 18−26.
(18) Naganuma, T.; Nakao, M.; Ichikawa, K.; Utsumi, H. *J. Pharm. Soc. Jpn.* **2015**, *135*, 733−738.
(19) Hyodo, F.; Naganuma, T.; Eto, H.; Murata, M.; Utsumi, H.; Matsuo, M. *Free Radical Biol. Med.* **2019**, *134*, 99−105.
(20) Eto, H.; Tsuji, G.; Chiba, T.; Furue, M.; Hyodo, F. *Free Radical Biol. Med.* **2017**, *103*, 209−215.
(21) Kawano, T.; Murata, M.; Hyodo, F.; Eto, H.; Kosem, N.; Nakata, R.; Hamano, N.; Piao, J. S.; Narahara, S.; Akahoshi, T.; Hashizume, M. *Sci. Rep.* **2016**, *6*, 32604.
(22) Grucker, D.; Chambron, J. *Magnet. Reson. Imag.* **1993**, *11*, 691−696.
(23) Eto, H.; Hyodo, F.; Nakano, K.; Utsumi, H. *Anal. Chem.* **2016**, *88*, 2021−2027.
(24) Fadda, A.; Barberis, A.; Sanna, D. *Food Chem.* **2018**, *240*, 174−182.
(25) Fontmorin, J. M.; Burgos Castillo, R. C.; Tang, W. Z.; Sillanpää, M. *Water Res.* **2016**, *99*, 24−32.
(26) Eto, H.; Hyodo, F.; Kosem, N.; Kobayashi, R.; Yasukawa, K.; Nakao, M.; Kiniwa, M.; Utsumi, H. *Free Radical Biol. Med.* **2015**, *89*, 1097−1104.
(27) Brayton, C. F. *Cornell Vet.* **1986**, *76*, 61−90.
(28) Britigan, B. E.; Rosen, G. M.; Chai, Y.; Cohen, M. S. *J. Biol. Chem.* **1986**, *261*, 4426−4431.
(29) Ueno, I.; Kohno, M.; Mitsuta, K.; Mizuta, Y.; Kanegasaki, S. *J. Biochem.* **1989**, *105*, 905−910.
(30) Ayer, A.; Gourlay, C. W.; Dawes, I. W. *FEMS Yeast Res.* **2014**, *14*, 60−72.
(31) Pisoschi, A. M.; Pop, A. *Eur. J. Med. Chem.* **2015**, *97*, 55−74.
(32) Iijima, H.; Tamura, G.; Hsiue, T. R.; Liu, Y.; Taniguchi, H.; Shirato, K. *Am. J. Resp. Crit. Care Med.* **1999**, *160*, 331−335.

(33) Zhao, G. D.; Yokoyama, A.; Kohno, N.; Sakai, K.; Hamada, H.; Hiwada, K. *Int. Arch. Allergy Immunol.* **2000**, *121*, 116−122.
(34) Matsumoto, K.; Hayakawa, H.; Ide, K.; Suda, T.; Chida, K.; Hashimoto, H.; Sato, A.; Nakamura, H. *Respirology* **2002**, *7*, 201−207.
(35) Izumi, Y.; Nakashima, T.; Masuda, T.; Shioya, S.; Fukuhara, K.; Yamaguchi, K.; Sakamoto, S.; Horimasu, Y.; Miyamoto, S.; Iwamoto, H.; Fujitaka, K.; Hamada, H.; Hattori, N. *Free Radical Biol. Med.* **2019**, *136*, 52−59.
(36) Fukuhara, K.; Nakashima, T.; Abe, M.; Masuda, T.; Hamada, H.; Iwamoto, H.; Fujitaka, K.; Kohno, N.; Hattori, N. *Free Radical Biol. Med.* **2017**, *106*, 1−9.
(37) Ogawa, Y.; Kubota, K.; Ue, H.; Kataoka, Y.; Tadokoro, M.; Miyatake, K.; Tsuzuki, K.; Yamanishi, T.; Itoh, S.; Hitomi, J.; Hamada, N.; Kariya, S.; Fukumoto, M.; Nishioka, A.; Inomata, T. *Int. J. Oncol.* **2009**, *34*, 609−618.
(38) Ogawa, Y. *Cancers* **2016**, *8*, E28.
(39) Aoyama, N.; Ogawa, Y.; Yasuoka, M.; Ohgi, K.; Iwasa, H.; Miyatake, K.; Yoshimatsu, R.; Yamanishi, T.; Hamada, N.; Tamura, T.; Kobayashi, K.; Murata, Y.; Miyamura, M.; Yamagami, T. *Oncol. Lett.* **2017**, *13*, 4741−4747.
(40) Miyatake, K.; Kubota, K.; Ogawa, Y.; Hamada, N.; Murata, Y.; Nishioka, A. *Oncol. Rep.* **2010**, *24*, 1161−1168.
(41) Aoyama, N.; Ogawa, Y.; Yasuoka, M.; Iwasa, H.; Miyatake, K.; Yoshimatsu, R.; Yamanishi, T.; Hamada, N.; Tamura, T.; Kobayashi, K.; Murata, Y.; Yamagami, T.; Miyamura, M. *Oncol. Lett.* **2017**, *13*, 69−76.

https://dx.doi.org/10.1021/acs.analchem.0c02331
Anal. Chem. XXXX, XXX, XXX−XXX